Climatological Study of Extreme Wind Events in a Coastal Area

Damyan Barantiev, Ekaterina Batchvarova, Hristina Kirova, and Orlin Gueorguiev

Abstract Long-term sodar measurements (Aug 2008–Oct 2016) of wind and turbulence profiles with high spatial (10 m) and temporal (10 min) resolution were performed at the southern Bulgarian Black Sea coast. This data has provided an opportunity to define "rare" values of meteorological parameters within their statistical distributions and to identify them as extreme events according to the Intergovernmental Panel on Climate Change. The statistical analysis of wind speed profiles has been performed for the eight-year period using the two parameter Weibull distribution. The determination of the ninety-percentile of this statistical distribution (at every sodar measurement level from 30 up to 600 m) has given values ("rare" events) that have defined the theoretical extreme wind speed profile (reference profile). On this basis, the extreme profiles during the reviewed period have been determined. Analysis of the distribution of the situations with extreme weather events by months and hours for the entire period has been performed. The multiple time series with the registered extreme profiles have been used to derive averaged parameters defining the vertical structure of the coastal boundary layer during extreme events. The thermodynamic state of the coastal boundary layer according to the Pasquill-Gifford classification has been revealed.

Keywords Sodar · Wind profiles · Turbulent characteristics · Extreme events · Black sea · Coastal PBL · Weibull distribution · Climatological study

1 Introduction

The society requires increased accuracy in time and space of forecasts; of observation data; of early warnings for dangerous and extreme weather events; and of climate

D. Barantiev (✉) · E. Batchvarova
Climate, Atmosphere and Water Research Institute, Bulgarian Academy of Sciences (CAWRI—BAS), 66, Tsarigradsko Shose blvd, Sofia 1784, Bulgaria
e-mail: dbarantiev@cawri.bas.bg

H. Kirova · O. Gueorguiev
National Institute of Meteorology and Hydrology (NIMH), 66, Tsarigradsko Shose blvd, Sofia 1784, Bulgaria

N. Dobrinkova and G. Gadzhev (eds.), *Environmental Protection and Disaster Risks*, Studies in Systems, Decision and Control 361,
https://doi.org/10.1007/978-3-030-70190-1_5

models' predictions in order to plan the future of the Planet. During the last years, many governments invest in the development of effective systems for observations and forecasting of hazardous meteorological events for prevention of socio-economic lost through adequate management and reduction of risks. The extreme phenomena and the specific thresholds for the extreme values of a corresponding climatic variable (e.g. wind speed), by definition, vary from place to place for natural reasons (different climates), because the extreme value of given meteorological parameter at one place, can be within the normal range at another place. A reason to apply different values is their application to socio-economic activities and needs, which also differ with climate. Despite their rarity, the extreme weather events are of a dangerous nature and could be harmful to human health, infrastructure, economy and even cause loss of human life [1, 2].

The advancement in ground-based remote sensing (*GBRS*) instruments proved them to be a tool to achieve more accurate spatial, qualitative and quantitative assessments of the processes within the planetary boundary layer (*PBL*). Information about an object or phenomenon is acquired without making physical contact and allows data to be collected for hazardous or inaccessible areas by remote sensing [3].

The capabilities of *GBRS* instruments to detect extreme wind events have been explored within the frame of SafeWind project at the Danish National Test Center for Large Wind Turbines at Høvsøre, Denmark [4]. Measurements in flat coastal terrain from two different types of lidars (continuous wave and a pulsed lidar) and a reference 116.5 m tall meteorological mast with cup anemometers were used for analysis of cup-lidar data comparisons in the experimental campaign. Wind data taken at 40, 60, 80 and 100 m above the ground showed that both lidars are capable for the maximum wind speed (*WS*) value determination within a 10-min averaging period up to an underestimation of about 10% with respect to the cup anemometers. Moreover, the probability density function (*PDF*) and the cumulative distribution function (*CDF*) of the time difference of the maximum *WS* between different instruments have been studied and comparisons of the gust factor have been discussed too. The experimental data showed better results for the pulsed lidar measurements with the same maximum at about 50% of the time and a comparable gust factor to that of the cup anemometers.

In Gottschall et al. [5], measurements results from a 100 m tall reference meteorological mast and two pulsed Doppler wind lidar units (one mounted on a floating table simulating motions of different possible offshore platforms and the other used as fixed reference instrument) were studied. In addition, based on the undisturbed wind data motion compensation algorithms were developed allowing correction of the affected measurement. Thus, the possibilities of the wind lidar mounted on a floating platform to determine properly turbulence as well extreme wind events were discussed. The results from the experimental campaign at the test site Tauche near Berlin showed that the 10-min mean values of horizontal *WS* agree quite well between both lidars but the turbulence intensity, as well as the recorded extreme wind values and the gust factors within a 10-min period values of the tilted lidar, was increased with respect to the fixed reference one. The developed compensation algorithm allowed to assess and control the impact of the motions of the floating platform.

A month of remote sensing data (April 2001) with high spatial and temporal resolution from Doppler sodar (DSDPA.90-24 METEK make) was used to describe the *WS* values in an extensive plateau (horizontal homogeneity area) in the North of Spain at the Low Atmosphere Research Centre (CIBA) [6]. This work included analysis of hourly means, daily *WS* evolution, *WS* power law, *WS* distribution by 10-min means of four *WS* classes, wind roses characteristics at 100 m for light and moderate winds, and four methods of fitting the two-parameter Weibull distribution function—linear regression by cumulative frequency, moments, maximum likelihood and quartiles. The results showed a sharp contrast between day and night cycle of *WS* due to strong convection during the day and the stratification stability during the night. Wind distribution revealed two prevailing directions at the frequent moderate winds considering synoptic forces affecting the Iberian Peninsula at the time of the measurements campaign. The close values of calculated Weibull parameters by the four different methods approved their usefulness for wind data analysis and practical purposes. A Radio Acoustic Sounding System (*RASS*) extension of the sodar provided temperature profiles. All sodar and RASS data were compared with meteorological mast measurements (10 min averages of temperature, *WS*, and wind direction at 100 m height and only temperature at 51 m) in Pérez et al. [7]. The results showed good comparability of sodar *WS* and RASS temperature measurements with those from the mast with satisfactory linear regression. For the wind direction measurements, statistical treatment of circular data was used and satisfactory correlation calculated by means of a nonparametric statistical test was obtained.

Such type of equipment is reliable and irreplaceable for a number of studies and innovative scientific methods of research on the mean meteorological parameters and turbulence in the *PBL* [8–14]. Over the past decade an integration of a number of *GBRS* devices within a uniform European network for observations was initialized through research and collaboration within several COST Actions: COST Action (EG-CLIMET) ES0702, COST Action 720, COST Action (TOPROF) ES1303 and COST Action (PROBE) CA18235 [12, 15–18]. Through the development of the necessary calibration standards for *GBRS* instruments, the establishment of procedures for maintenance and automatic control of data quality, common data formats, and protocols for exchange of data, these COST actions aim at standardization of the use of *GBRS* data for better weather forecast and thus to increase of the quality of all meteorological products in service of society.

Unfortunately, the modern *GBRS* methods are not developed in operational mode in Bulgaria, though such data are needed for fundamental theoretical research, climatological studies, evaluation of meteorological models, economic and air quality activities.

2 Study Area, Experiment Equipment, and Data Overview

2.1 Measuring Side

Data collection and analysis in the coastal *PBL* using acoustic sounding starts in Bulgaria from the summer of 2008 at the Meteorological Observatory (MO) Ahtopol, located on the coast of south-eastern Bulgaria (Fig. 1—yellow pin). These high special and temporal resolution measurements allow to start climatological studies of the coastal *PBL* in Bulgaria [19–22]. The climatic zoning of Bulgaria presented in Sabev, Stanev [23] attributed the studied area into the Black Sea coastal Strandzha climate region, which is under the influence of the Black Sea climatic sub region of the Continental-Mediterranean climate zone in Bulgaria. Typically, in this climate region, well expressed breeze circulation in the warm part of the year is observed, whereas during the cold part of the year a lower frequency and smaller time and spatial scales of the coast circulation is registered [24]. MO Ahtopol is located on a flat grassy terrain at 30 m height above sea level and at about 400 meters inland. The shore near the observatory is steep, about 10 meters high cliffs and the coastline stretches from north-northwest to south-southeast (Fig. 1).

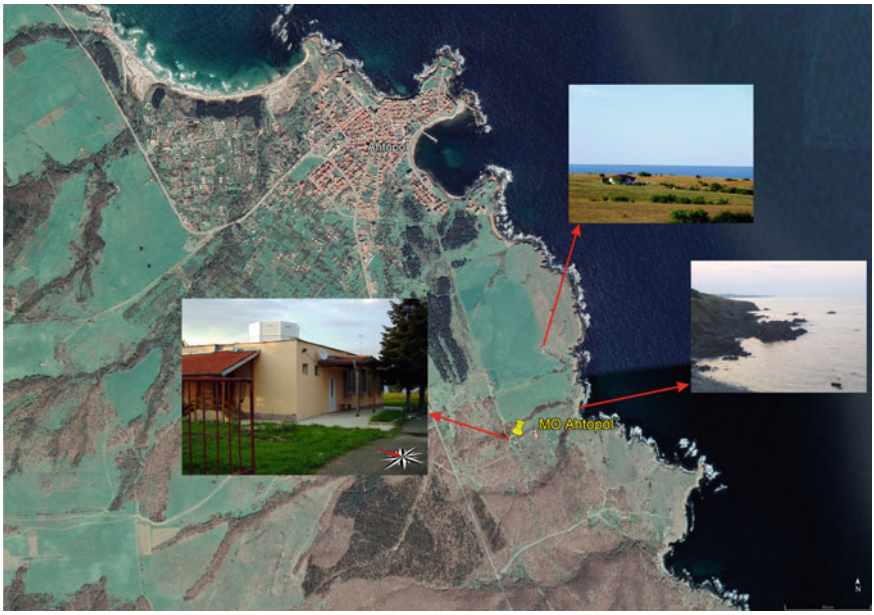

Fig. 1 Location of MO Ahtopol in Bulgaria on Google Earth (42° 5′ 3.37″ N, 27° 57′ 4.49″ E) with views of the terrain (right) and sodar system on the roof of the administrative building of MO Ahtopol (left)

2.2 Measuring Instrument Used

To study the wind and turbulence profiles in coastal *PBL*, a multibeam acoustic monostatic Doppler system for sounding the atmosphere is used—SCINTEC Flat Array Sodar MFAS with frequency range 1650–2750 Hz, 9 angles of emission/reception (0°, ±9.3°, ±15.6°, ±22.1°, ±29°), vertical range from 150 to 1000 m, with 10 m resolution, first level of measurement 30 m. The accuracy for *WS* is 0.1–0.3 ms^{-1}, and for the wind direction is 2°–3° [25].

The sodar system is installed on the roof of the administrative building of the MO Ahtopol (Fig. 1) at an approximate height of 4.5 m. During the study period its settings undergo a number of changes, mainly related to the update of the operation software. Thanks to these changes, more reliable operation is achieved during atmosphere sounding and its vertical range is increased while maintaining the data resolution. The basic settings do not undergo significant changes and the quality control of the data is maintained, as throughout the period the sodar records every 10 min with averaging period of 20 min (running averages) with a vertical resolution of 10 m. Due to the operating software updates over the years, the vertical range of the sodar in 2008 reached 520 m in height, while in 2016 it was 1000 m. In summary, the effective sodar range (the height to which wind profiles are measured) depend mainly on the turbulent inhomogeneities in the atmosphere, on the spatial and temporal resolution setup and operational software updates.

2.3 Data Availability

In this work we explore 3014-day period (1 August 2008–31 October 2016) of acoustic soundings in the coastal *PBL* with 341,971 profiles corresponding to 78.8% time coverage. The monthly data availability and maximum effective height reached by the sodar are presented in Table 1. Data with availability below 40% is given in red, between 40 and 70% in yellow, and above 70% in green. The maximum vertical range for this study is set to 600 m due to the lower data availability above this height. The actual sodar range is also presented graphically in Table 1 with filled bars at a height—over 810 m (4 bars), over 710 m (3 bars), over 610 m (2 bars).

The continuity of the operation of the sodar during the study period was disturbed by frequent accidents of the main power supply on the territory of the MO Ahtopol until 2011 (Table 1—yellow and red colors). During the second half of 2008 and 2009, the sodar was stopped during the night hours. From 1st August to 31st October 2008 the measurements were made in the daytime, from 7:00 a.m. to 6:00 p.m. From 8th December 2008 to 27th July 2009 the sodar worked continuously and after that until December 2009 only during the day, from 7:30 a.m. to 9:40 p.m. After December 2009 the sodar functioned with no restrictions. The operational data records from the sodar until 26 September 2014 were made in local time (i.e. during the cold half of the year/UTC + 2/, and during the warm half/UTC + 3/). After this period, the

Table 1 Data availability from the acoustic sounding of the atmosphere and maximum effective height reached during the study period on the territory of the MO Ahtopol

	I	II	III	IV	V	VI	VII	VIII	IX	X	XI	XII
2008	-	-	-	-	-	-	-	45.2%	40.3%	57.7%	59.5%	88.4%
max range [m]	-	-	-	-	-	-	-	520	520	520	520	520
2009	99.9%	99.6%	99.2%	96.7%	98.3%	99.3%	94.6%	57.5%	59.9%	58.4%	96.7%	96.0%
max range [m]	520	520	680	680	680	680	680	680	680	680	680	680
2010	97.5%	98.3%	89.0%	68.5%	96.8%	86.4%	99.9%	98.3%	99.9%	92.6%	99.6%	99.8%
max range [m]	680	680	680	680	680	680	560	510	510	510	510	510
2011	96.8%	94.8%	99.8%	96.7%	96.8%	96.2%	92.2%	99.9%	38.8%	78.8%	99.2%	81.3%
max range [m]	510	460	510	510	510	510	510	510	560	620	620	620
2012	75.3%	95.8%	99.7%	96.7%	99.3%	93.3%	99.1%	31.9%	96.6%	30.6%	23.3%	100.0%
max range [m]	620	620	620	620	620	620	700	620	720	670	640	720
2013	96.6%	96.4%	50.6%	100.0%	98.3%	54.7%	95.3%	96.3%	96.7%	58.0%	74.7%	61.7%
max range [m]	720	720	720	620	680	670	680	680	720	720	720	720
2014	100.0%	99.9%	99.7%	100.0%	97.1%	99.8%	90.0%	59.4%	51.7%	98.5%	97.5%	98.0%
max range [m]	720	720	720	720	720	720	720	720	750	750	750	730
2015	99.9%	96.3%	94.9%	97.8%	69.5%	73.3%	57.4%	97.9%	99.5%	99.9%	65.9%	95.1%
max range [m]	750	750	750	750	750	750	590	750	750	750	750	730
2016	80.1%	70.0%	76.1%	49.9%	35.6%	93.2%	99.9%	93.0%	75.0%	45.4%	-	-
max range [m]	750	750	750	750	750	1000	1000	1000	1000	750	-	-

sodar data were recorded only in winter time, i.e. UTC + 2. Most of the analyses performed in this work are independent of the time, but for the needs of the extreme weather events distribution analysis by month and hour for the entire period, the entire time series is converted to UTC + 2.

3 Methodology

The analysis for extreme winds is related to the derivation of a theoretical extreme profile (reference profile) of the *WS* on the basis of which the extreme speed profiles are determined. For this purpose, an analysis of the *WS* distribution in height was performed by processing the values of *WS* for each individual profile both in height (every 10 m) and in *WS* intervals from 0 to 40 ms^{-1} through 1 ms^{-1} as follows:

- calm—at values of *WS* > or = 0 ms^{-1}, but < 0.5 ms^{-1}
- interval 1 ms^{-1}—at values of *WS* > or = 0.5 ms^{-1}, but < 1.5 ms^{-1}
- interval 2 ms^{-1}—at values of *WS* > or = 1.5 ms^{-1}, but < 2.5 ms^{-1}
- …
- interval 40 ms^{-1}—at values of *WS* > or = 39.5 ms^{-1};

The *WS* probability distribution for all *WS* profiles measured at MO Ahtopol is obtained by histograms at each level with applied *PDF* also known as the two parameter Weibull distribution [26] described in Eq. (1) based of the method of maximal likelihood [27]. The two distribution parameters are given in Eqs.: (2) and (3) [28], respectively, for a shape parameter $\hat{k}$,which has a non-dimensional value defining the shape of the probability density distribution curve and the scale parameter $\hat{c}$ assuming the dimension of the variable and representing the 63.2th percentile of the distribution [29].

$$f(u;c,k)=f(x)=\begin{cases}\frac{k}{c}\left(\frac{u}{c}\right)^{k-1}e^{-(u/c)^k}, & u\geq 0\\ 0, & u<0\end{cases} \tag{1}$$

$$\hat{k}^{-1}=\frac{\sum_{i=1}^{N}\left(u_i^k\ln u_i-u_N^k\ln u_N\right)}{\sum_{i=1}^{N}\left(u_i^k-u_N^k\right)}-\frac{1}{N}\sum_{i=1}^{N}\ln u_i \tag{2}$$

$$\hat{c}^k=\frac{1}{N}\sum_{i=1}^{N}\left(u_i^k-u_N^k\right) \tag{3}$$

The two-parameter Weibull distribution is one of the most commonly used and preferred distributions in wind potential estimates and has been studied in a number of scientific papers [30–34]. In this study we use it to employ the definition of the Intergovernmental Panel on Climate Change [1, 35] for extreme events (exceedance over a relatively low threshold) through determination of the 90th percentile of the performed statistical distribution for all heights. Thus, the "reference" values, at/above which the *WS* is considered as extreme, are defined.

In this way, "reference" wind profile is derived and extreme wind events are determined by comparing it with the actual profiles during the study period. Only profiles with at least ten points with values equal to or greater than those of the reference profile are used. Finally, an "extreme wind "data set based on sodar data is created containing 10,854 extreme wind profiles representing about 3.2% of the soundings performed.

4 Results

WS histograms with applied Weibull distributions, certain 90th percentile and statistical data for different measurement levels for the study period in Ahtopol are shown in Fig. 2.

The pink bar, on the side of each histogram, is indicator for data availability at each of the displayed levels. The number of measurements involved in the derivation of the statistical graphs in Fig. 2 decreases sharply in height due to the lower number of profiles reaching the corresponding level of measurement. At 50 m (Fig. 2—top left), a 99.2% data availability is achieved, while at 350 m (Fig. 2—bottom left) this value is already 35%, and at 550 m (Fig. 2—bottom right) only 4.4%, which is equal to just over 15,000 profiles reaching this height. A characteristic change with height of the *WS* histograms is observed, which is expressed by the typical shift of the maximum to higher *WS* values. The highest probability (nearly 27%) is observed at winds falling in the interval defined as 1 ms^{-1} at 50 m above the ground level (*AGL*), while at 550 m there are two pronounced maxima determined by the intervals 4 and 11 ms^{-1} (about 8% of cases for each interval). Due to the larger variability of *WS* with height, a "widening" of the graphs in the Weibull distributions applied to the respective histograms (Fig. 2—red curves) and in the histograms themselves is

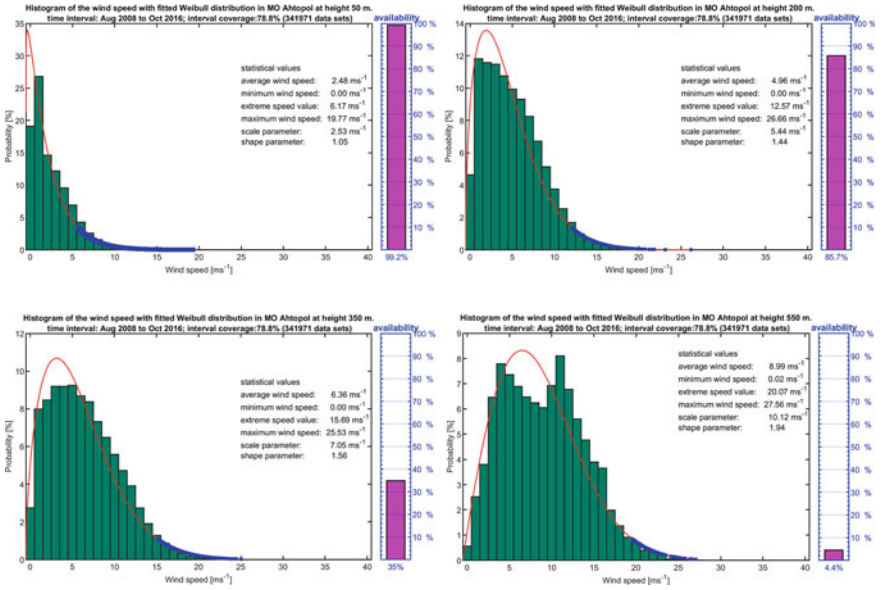

Fig. 2 Histograms of *WS* (green bars), two-parameter Weibull distributions (red curves), certain values equal to or exceeding the 90th percentile of the probability density of Weibull distributions (blue squares), availability of data (pink bar) and derived statistical data. Top left—level 50 m, top right—200 m, bottom left—350 m, bottom right—550 m

observed (Fig. 2—green bars). The extent to which the Weibull distribution graph is "shrunk" is determined by the shape parameter $\hat{k}$ (2)—the larger value corresponds to more "wider" distribution graph. For each Weibull distribution, actual measured values equal to or greater than its 90th percentile (blue squares on the red curve) are presented, which according to the IPCC definition are defined as extreme values of *WS* [1, 35]. In addition, to each of the graphs in Fig. 2 statistical values for the respective heights are derived, such as minimum, maximum and average values of *WS*, extreme value determined by the 90th percentile, as well as values of the two parameters of the respective Weibull distribution.

By summarizing the information presented in Fig. 2 from 30 to 600 m *AGL* with 10 m resolution the changes in the probability distributions of *WS* in height with the attached "reference" profile of extreme values of *WS* (minimum extreme values—determined by the 90th percentile of statistical distributions in height) for the whole considered period are obtained and presented at Fig. 3.

The color bar shows the probability distribution values changes in height, as its color range is limited to 10% in order to achieve better visualization of the results (values of probability distributions above 10% are colored as 10%, but values under 0.2% are still not viewable). The area with maximum values of the probability distribution of *WS* in height is clearly observed at the presented graph, as up to 170 m the probability is highest for *WS* up to 3 ms^{-1}. At 300 m, high probability is observed in

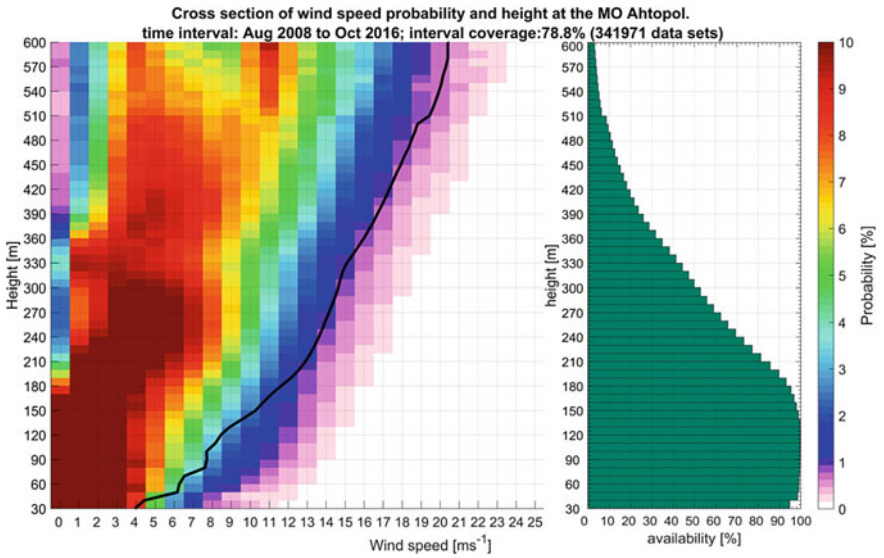

Fig. 3 Diagram of *WS* probability distributions at different heights (color section of altitude and speed intervals) with available data (green bars) and applied reference profile for extreme values of *WS* (black profile), determined by the 90th percentile of the statistical distributions in height

winds of 3 to 6 ms^{-1}. At 600 m the probability is highest for winds speeds 4–5 ms^{-1} and 10–12 ms^{-1}. From the green bars showing the change in the number of profiles reaching a certain height, it can be seen that their availability begins to decrease sharply after 180 m *AGL*, with a maximum of data observed in the layer from 90 to 140 m. Almost 5% lower data availability is observed at the first level of the sodar measurements (30 m *AGL*) than the layer at which the maximum data is. The values of the reference extreme WS profile (*REWSP*) (Fig. 3—black profile) increase with height, as the extreme values at 30 m *AGL* are about 4 ms^{-1}, and at 600 m—about 20 ms^{-1}. Close to the ground, where the availability of data is significant, two small peaks are observed in the reference profile (at heights of 50 and 80 m), differing against the background of gradually increasing extreme values in height. These relatively sharp changes in the reference values determined by the 90th percentile of the respective statistical distributions can be associated with corresponding changes of the probability density curve shape of the Weibull distribution graphs at these heights, expressed respectively by relevant changes in the shape parameter. *REWSP* is located primarily in the area with a probability distribution of *WS* between 1 and 4% up to 200 m and between 1 and 2% higher up. This may be associated with the typically larger and more varied presence of higher *WS* in height, leading to lower values and shifting the maximum of the probability distribution to higher speed ranges. At least 50% probability is available in total for the first two speed intervals (calm and 1 ms^{-1}) up to 40 m *AGL* due to which relatively low values of *REWSP* close to the surface are observed.

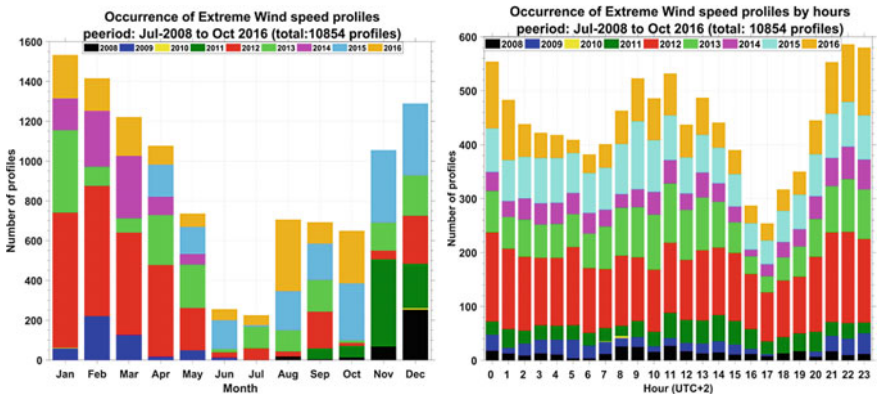

Fig. 4 Number of extreme wind speed profiles reported during the different years of the study at MO Ahtopol by month (left) and hour of the day (right)

The number of extreme wind speed profiles during the different years of the study period by month and hour of the day is shown in Fig. 4.

The number of extreme wind speed profile (*EWSP*) for the period is 10,854 or 3.2% of all profiles included in the statistics. It can be noted that 2012 (Fig. 4—red) was the windiest year (excluding 2008 and 2016 for which the data do not cover a calendar year). In 2010 only 13 *EWSP* were registered in December around 8 a.m. The intensity of the atmospheric circulation dynamics, over the studied area, is evident from the variability of the number of profiles during the different months and hours of the day. *EWSP* are observed in all months and hours, and the maxima can be localized in the cold half of the year and during the day when the processes in the atmosphere are more intense. The biggest number of extreme profiles (over 1500) is observed in January, and the calmest months are June and July, when the number of extreme profiles is just over 200. Calm and windy periods at Ahtopol can be also identified, namely July 2009–August 2011 was a calm period, while September 2011–June 2014 and April 2015–October 2016 were windy periods. Calmer periods are revealed at 6-7 a.m. and 5-6 p.m., which are related to the start and end of the day during cold seasons (when a bigger number of *EWSP* are reported) and calm periods in the beginning and end of sea breeze during warm seasons. Most windy are the periods 10 p.m.–1 a.m. and 11 a.m.–1 p.m., which can be related to the maximal development of the local circulation in both directions.

The vertical structure of the coastal *PBL* in the study area during extreme winds phenomena is presented in Fig. 5 by averaged profiles and their dispersions of 12 output parameters from the sodar measurements—from left to right and from top to bottom: wind direction (*WD*), extreme wind speed profile (*WS*), extreme speed profile dispersion (*sigWS*), vertical wind speed (*W),* vertical wind speed dispersion (*sigW*), horizontal (western) component of the extreme profile (*U*), dispersion of the western component (*sigU*), horizontal (southern) component of the extreme profile (*V*), dispersion of southern component (*sigV*), eddy dissipation rate (*EDR*), turbulent

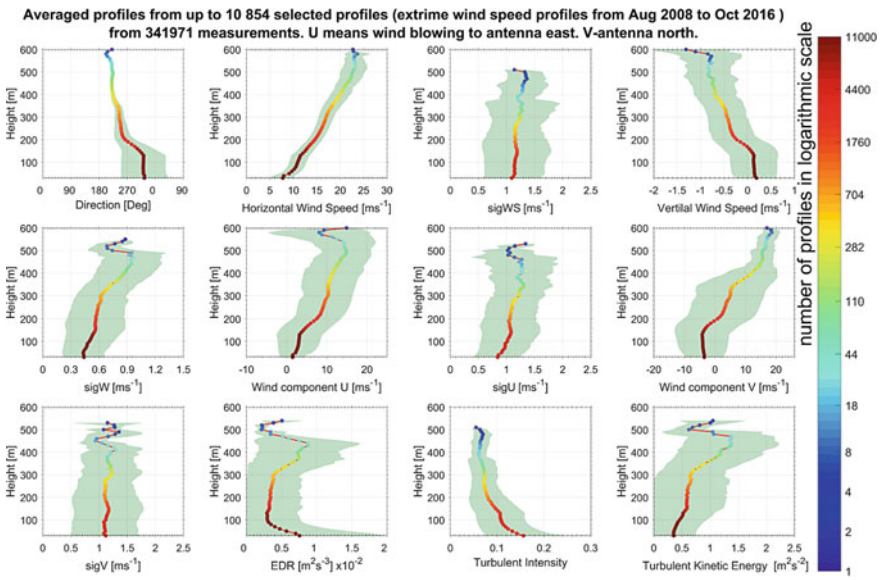

Fig. 5 Averaged profiles and their dispersions from a sample with a maximum of 10 854 selected extreme wind speed profiles

intensity (*TI*) and turbulent kinetic energy (*TKE*). Different number of values are used for the derivation of the average values at different measurements levels. The color bar (on the right side of the graphs) shows the number of profiles involved in calculations of the averaged values and their dispersions at a certain level, as it is on a logarithmic scale for better visualization of the results due to the lower availability of profiles in height.

The *WD* profile graph (Fig. 5) shows north-northwest direction in the registered extreme winds up to 130 m (where most of the profiles are concentrated), which is related to wind blowing parallel to the coastline. Gradual change to west direction is observed between 130 and 200 m. Higher up, the *WD* is southwesterly. The greatest dispersion of this profile is observed in the first 130 m, after which it decreases gradually. The averaged extreme wind speed profile (*EWSP)* is characterized by a relatively constant dispersion in height, and an almost linear increase in values. Velocities from 8 to 12 ms^{-1} up to 130 m, and their rapid increase in height reaching values close to 24 ms^{-1} up to 600 m are observed. In the profile of *W*, positive values up to 160 m altitude are observed, after which negative values are recorded decreasing to -1.3 ms^{-1} at 600 m. In almost all presented averaged profiles, changes in the profiles shape in the layer 40–60 m are observed. In the *EDR* profile a sharp decrease of the values up to 90 m is observed. Also, of interest is the *sigW* profile with slight peak at a height of 150–160 m (where a sharper change of *WD* and faster decrease of the *W* values are observed), followed by almost constant values up to 300 m, and an increase up to the second main peak between 440 and 490 m. At this

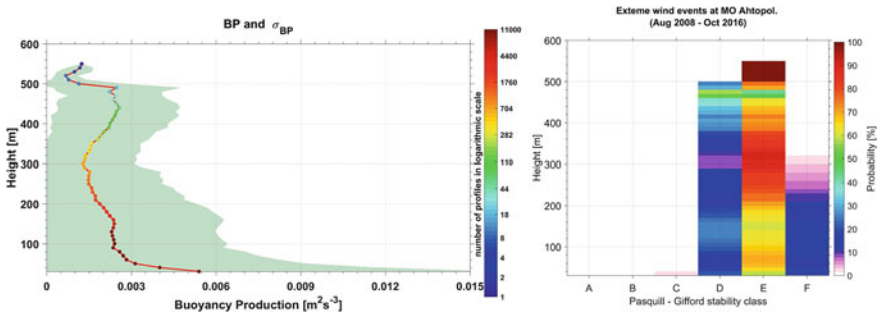

Fig. 6 Averaged Buoyancy Production profile (left) and diagram of stability classes probabilities at different heights (right) during extreme wind events from Aug 2008 to Oct 2016

height *sigW* reaches maximum values. These peaks are also reflected in the shape of the other averaged turbulent profiles.

Following Illingworth et al. [12] the *PBL* height at Ahtopol during extreme wind situations is between 440 and 490 m. The height with peculiarities in the profiles in Fig. 5 of 40–60, 90 and 150 m can be related to Internal Boundary Layer (*IBL*) and surface layer (*SL*) heights, or very low nocturnal *PBL* height in cold seasons.

Two more parameters characterizing the structure of the coastal boundary layer are shown in Fig. 6. In the left graph the averaged profile of Buoyancy Production (*BP*) is presented considering its active role in the TKE production and momentum transfer. The involved *BP* profiles in the averaging are obtained using the dispersion of the vertical wind speed *sigW* (σ_w) profiles derived from sodar at different altitudes (z) with Eq. (4) [8]:

$$\beta = \frac{\sigma_w^3}{z} \tag{4}$$

In the *BP* profile a sharp decline in the values in the first 90 m followed by almost constant values up to 130 m and two peaks (slight at 150 m and main between 440 and 490 m) coinciding in height with the peaks of *sigW* and *TKE* are observed. In general, the average Archimedes force decreases in height, with the maximum values observed near the ground (where the turbulent heat flow is maximum) and the minimum in the extreme high parts of the average profile. A diagram of stability classes probabilities at different heights is shown in Fig. 6 (right). The profiles of atmospheric stability classes according to the Pasquill-Gifford classification using the σ_ϕ method [36] are used as an additional output from the sodar measurements to retrieve the thermodynamic state of the atmosphere during extreme wind events. Only time series with available stability classes data at respective altitude are used for the consideration of the 100% probability.

The dominant class of atmospheric stratification can be indicated as the slightly stable (E) with more than 50% probability almost throughout the acoustic sounding layer and with 100% probability after 500 m. The next dominant class according to the

Pasquill-Gifford classification used is neutral (D) with probability distribution values in the range between 9 and 58%. About 20% of averaged probability distribution is registered as D stability class for the whole measurement layer while for the E stability class 66% can be pointed as averaged probability distribution with minimum value of about 42% at 470 m. The stable stratification (F) is presented with maximum value of about 18% close to the surface and with averaged probability distribution of about 13% for the entire layer. The probability distributions of the other three classes of atmospheric stability are present with very low values close to the surface, which is the reason why only weakly unstable class (C) is visualized in the right graph of Fig. 6 with maximum value about 2% and averaged about 0.2%. The maximum values of moderately (B) and extremely unstable (A) classes have been below 0.2%.

5 Conclusions

The derived averaged characteristics of the coastal *PBL* in extreme winds conditions are pioneering result based on unique set of *GBRS* observation data at a Bulgarian Black Sea coastal site. In this paper a super position of different types of air masses is considered which allows to assess the vertical structure and height of the *PBL* (determined between 440 and 490 m by the main peaks at graphs of *sigW*, *EDR* and *TKE* in Fig. 5 and graph of *PB* in Fig. 6), the *IBL* height of 40–60 m at high winds and *SL* height or very low nocturnal *PBL* height in cold seasons of 90 or 150 m. The dominant thermodynamic state of the coastal boundary layer according to the Pasquill-Gifford classification can be characterized as slightly stable (E) with averaged probability distribution of 66% for the whole measurement layer followed by neutral (D) stratification with 20% and stable stratification (F) with 13%. This climatic study reveals that quiet and windy periods can be of different length, which is likely related to different types of prevailing weather structures. The observed winter highs and summer lows of extreme winds are likely due to the presence of local coastal circulation. The distinct morning and evening lows in the average distribution by hour are related to transitions between night and day and start or end of sea breeze. The distribution of EWSP by year, month and hour of the day is important climatological feature, which is of great use for economic activities (such as construction of buildings, wind energy potential, air quality, climate comfort for citizens and tourists, etc.) and municipal emergency plans and actions in cases of meteorological extreme phenomena. The methodology used in this study is suitable for variety of remote sensing instruments with long-term data sets, while allowing both the evaluation of diagnostic or prognostic numerical models under extreme events conditions and integration into synergy systems for monitoring, control and robust decision making in the challenge of increasing climate change rates in recent years.

Acknowledgements The work is within the frame of research projects DM 14/1 26-05-2020 (REPLICA—extReme Events and wind ProfiLe In a Coastal Area) project, funded by National

Science Fund of Bulgaria and it was partially supported by the Bulgarian Ministry of Education and Science under the National Research Programme "Young scientists and postdoctoral students" approved by DCM # 577 /17.08.2018. The contribution of E. Batchvarova is supported by the National Science Fund of Bulgaria, Contract KP-06-N34/1 30-09-2020 "Natural and anthropogenic factors of climate change—analyses of global and local periodical components and long-term forecasts".

References

1. IPCC: Climate Change 2001: The Scientific Basis. Contribution of Working Group I to the Third Assessment Report of the Intergovernmental Panel on Climate Change. In: Houghton, J.T., Ding, Y., Griggs, D.J., Noguer, M., van der Linden, M., P.J., Dai, X., Maskell, K., Johnson, C.A. (eds.). p. 881. Cambridge University Press, United Kingdom and New York, NY, USA (2001)
2. IPCC: Managing the Risks of Extreme Events and Disasters to Advance Climate Change Adaptation. A Special Report of Working Groups I and II of the Intergovernmental Panel on Climate Change. In: Field, C.B., Barros, V., Stocker, T.F., Dahe, Q., Dokken, D.J., Ebi, K.L., Mastrandrea, M.D., Mach, K.J., Plattner, G.-K., Allen, S.K., Tignor, M., Midgley, P.M. (eds.). Cambridge University Press, Cambridge, UK, and New York, NY, USA (2012)
3. Prasad, S.T.: Remotely Sensed Data Characterization, Classification, and Accuracies Remote Sensing Handbook, vol. 1. CRC Press, (2015)
4. Sathe, A., Courtney, M., Mann, J., Wagner, R.: How good are remote sensors at measuring extreme winds?. Paper presented at the EWEA Conference, Brussels, Belgium, 14–17 March 2011
5. Gottschall, J., Wolken-Möhlmann, G., Lange, B.: About offshore resource assessment with floating lidars with special respect to turbulence and extreme events. J. Phys. Conf. Ser. **555**(1), 012043 (2014). https://doi.org/10.1088/1742-6596/555/1/012043
6. Pérez, I.A., García, M.A., Sánchez, M.L., de Torre, B.: Analysis of height variations of sodar-derived wind speeds in Northern Spain. J. Wind Eng. Ind. Aerodyn. **92**(10), 875–894 (2004). https://doi.org/10.1016/j.jweia.2004.05.002
7. Pérez, I.A., Sánchez, M.L., García, M.A., de Torre, B.: Comparison between measurements obtained with a meteorological mast and a RASS sodar. In: 3rd International Conferences on Experiences with Automatic Weather Stations, Torremolinos, Malaga, Spain, 19–21 Feb 2003
8. Engelbart, D., Monna, W., Nash, J., Mätzler, C.: COST 720 Final Report: Integrated ground-based remote-sensing stations for atmospheric profiling. Office for Official Publication of the European Communities, Luxembourg (2009)
9. Cimini, D., Marzano, F.S., Visconti, G.: Integrated Ground-Based Observing Systems. Springer, Berlin Heidelberg (2011)
10. Emeis, S.: Surface-based remote sensing of the atmospheric boundary layer, 1st ed. Atmospheric and Oceanographic Sciences Library. Springer Berlin Heidelberg, New York (2010)
11. Peña, A., Floors, R.R., Sathe, A., Gryning, S.-E., Wagner, R., Courtney, M., Larsén, X.G., Hahmann, A.N., Hasager, C.B.: Ten years of boundary-layer and wind-power meteorology at Høvsøre, Denmark. Bound.-Layer Meteorol. **158**(1), 1–26 (2016). https://doi.org/10.1007/s10546-015-0079-8
12. Illingworth, A., Ruffieux, D., Cimini, D., Lohnert, U., Haeffelin, M., Lehmann, V.: COST action ES0702 final report: European ground-based observations of essential variables for climate and operational meteorology. In: COST Action ES0702 EG-CLIMET, p. 141. COST Office, PUB1062 (2013)
13. Coulter, R.L., Kallistratova, M.A.: Two decades of progress in SODAR techniques: a review of 11 ISARS proceedings. Meteorol. Atmos. Phys. **85**, 3–19 (2004). https://doi.org/10.1007/s00703-003-0030-2

14. Bradley, S., Antoniou, I., Hünerbein, S.v., Kindler, D., Noord, M.d., Jørgensen, H.: SODAR calibration procedure (final reporting on WP3, EU WISE project NNE5-2001-297) In: Stuart Bradley, p. 69. The University of Salford, Salford, Greater Manchester, UK, (2005)
15. Engelbart, D., Monna, W., Nash, J., Mätzler, C.: Integrated ground-based remote-sensing stations for atmospheric profiling. In: Engelbart, D., Monna, W., Nash, J., Mätzler, C. (eds.), COST action 720: Final Report, p. 398. Publications Office of the European Union - COST Office, Luxembourg (2009)
16. Illingworth, A., Ruffieux, D., Haeffelin, M., O'Connor, E., Cimini, D., Potthast, R.: COST Action Final Achievement Report ES1303: Towards operational ground based profiling with ceilometers, doppler lidars and microwave radiometers for improving weather forecasts (TOPROF). In: Illingworth, A., Ruffieux, D., Haeffelin, M., O'Connor, E., CIMINI, D., Potthast, R. (eds.). COST Association AISBL, Brussels, Belgium, (2017)
17. Illingworth, A., Cimini, D., Gaffard, C., Haeffelin, M., Lehmann, V., Löhnert, U., O'Connor, E.J., Ruffieux, D.: Exploiting existing ground-based remote sensing networks to improve high-resolution weather forecasts. Bull. Am. Meteor. Soc. **96**(12), 2107–2125 (2015). https://doi.org/10.1175/BAMS-D-13-00283.1
18. Cimini, D., Haeffelin, M., Kotthaus, S., Löhnert, U., Martinet, P., O'Connor, E., Walden, C., Coen, M.C., Preissler, J.: Towards the profiling of the atmospheric boundary layer at European scale—introducing the COST Action PROBE. Bull. Atmos. Sci. Technol. **1**(1), 23–42 (2020). https://doi.org/10.1007/s42865-020-00003-8
19. Barantiev, D., Novitsky, M., Batchvarova, E.: Meteorological observations of the coastal boundary layer structure at the Bulgarian Black Sea coast. Adv. Sci. Res. (ASR) (6), 251–259 (2011). https://doi.org/10.5194/asr-6-251-2011
20. Batchvarova, E., Barantiev, D., Novitsky, M.: Costal boundary layer wind profile based on SODAR data—Bulgarian contribution to COST Acton ES0702. Paper presented at the The 16th International Symposium for the Advancement of Boundary-Layer Remote Sensing—ISARS Boulder, Colorado, USA, 5–8 June 2012
21. Novitsky, M., Kulizhnikova, L., Kalinicheva, O., Gaitandjiev, D., Batchvarova, E., Barantiev, D., Krasteva, K.: Characteristics of speed and wind direction in atmospheric boundary layer at southern coast of Bulgaria. Russ. Meteorol. Hydrol. **37**(3), 159–164 (2012). https://doi.org/10.3103/S1068373912030028
22. Barantiev, D., Batchvarova, E., Novitsky, M.: Exploration of the coastal boundary layer in ahtopol through remote acoustic sounding of the atmosphere. Paper presented at the 2nd National Congress on Physical Sciences and 41st National Conference on Physics Education Matters, Sofia, Bulgaria, 25–29 Sept 2013
23. Sabev, L., Stanev, S.: Climate regions of Bulgaria and their climate, vol. V. State Publishing House "Science and Art", Sofia, Bulgaria (1959)
24. Barantiev, D., Batchvarova, E., Novitsky, M.: Breeze circulation classification in the coastal zone of the town of Ahtopol based on data from ground based acoustic sounding and ultrasonic anemometer. Bulgarian J. Meteorol. Hydrol. (BJMH) **22**(5), 24 (2017)
25. ScintecAG: Scintec Flat Array Sodars - Hardware Manual (SFAS, MFAS, XFAS) including RASS RAE1 and windRASS, Version 1.03 ed. Scintec AG, Germany (2011)
26. Papoulis, A., Pillai, S.U.: Probability, Random Variables, and Stochastic Processes, 4th edn. McGraw-Hill Europe (2002)
27. Indhumathy, D., Seshaiah, C.V., Sukkiramathi, K.: Estimation of Weibull parameters for wind speed calculation at Kanyakumari in India. J. Innov. Res. Sci. Eng. Technol. **3**(1) (2014)
28. Sornette, D.: Critical Phenomena in Natural Sciences: Chaos, Fractals Selforganization and Disorder: Concepts and Tools. Springer, Berlin (2004)
29. Papanchev, T.: A modified approach for parameters estimation of the Weibull distribution for interval data and zero or few failures. J. Notices Union Sci. Varna, Technical Sciences Series (2013)
30. Gryning, S.-E., Batchvarova, E., Floors, R.R., Peña, A., Brümmer, B., Hahmann, A.N., Mikkelsen, T.: Long-term profiles of wind and Weibull distribution parameters up to 600 m in a rural coastal and an inland suburban area. Bound.-Layer Meteorol. **150**(2), 167–184 (2014). https://doi.org/10.1007/s10546-013-9857-3

31. Lun, I.Y.F., Lam, J.C.: A study of Weibull parameters using long-term wind observations. Renew. Energy **20**(2), 145–153 (2000). https://doi.org/10.1016/s0960-1481(99)00103-2
32. He, Y., Monahan, A.H., Jones, C.G., Dai, A., Biner, S., Caya, D., Winger, K.: Probability distributions of land surface wind speeds over North America. J. Geophys. Res. Atmos. **115**(D4) (2010). https://doi.org/10.1029/2008JD010708
33. Wijnant, I.L., van den Brink, H.W., Stepek, A.: North Sea Wind Climatology Part 1: A Review of Existing Wind Atlases, vol. TR-342, p. 66. Royal Netherlands Meteorological Institute Ministry of Infrastructure and the Environment, De Bilt, Netherlands, (2014)
34. Stevens, M.J.M., Smulders, P.T.: The estimation of the parameters of the Weibull wind speed distribution for wind energy utilization purposes. Wind Eng. **3**(2), 132–145 (1979)
35. IPCC: Climate Change 2007: Synthesis Report. Contribution of Working Groups I, II and III to the Fourth Assessment Report of the Intergovernmental Panel on Climate Change. In: Team, C.W., Pachauri, R.K., Reisinger, A. (eds.), p. 104. IPCC, Geneva, Switzerland, Printed in Sweden (2007)
36. Bailey, D.T.: Meteorological monitoring guidance for regulatory modeling applications. In: Standards, O.o.A.Q.P.a. (ed.), p. 171. United States Environmental Protection Agency (EPA), Research Triangle Park, NC 27711 (2000)